

PCCP

Accepted Manuscript



This is an *Accepted Manuscript*, which has been through the Royal Society of Chemistry peer review process and has been accepted for publication.

Accepted Manuscripts are published online shortly after acceptance, before technical editing, formatting and proof reading. Using this free service, authors can make their results available to the community, in citable form, before we publish the edited article. We will replace this *Accepted Manuscript* with the edited and formatted *Advance Article* as soon as it is available.

You can find more information about *Accepted Manuscripts* in the [Information for Authors](#).

Please note that technical editing may introduce minor changes to the text and/or graphics, which may alter content. The journal's standard [Terms & Conditions](#) and the [Ethical guidelines](#) still apply. In no event shall the Royal Society of Chemistry be held responsible for any errors or omissions in this *Accepted Manuscript* or any consequences arising from the use of any information it contains.



Journal Name

ARTICLE

Mechanochemistry of lithium nitride under hydrogen gas

Z. Li,^{a,b} J. Zhang,^a S. Wang,^b L. Jiang^b, M. Latroche,^a J. Du,^b and F. Cuevas^{a†}

Received 00th January 20xx,
Accepted 00th January 20xx

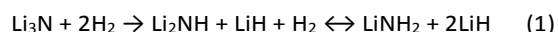
DOI: 10.1039/x0xx00000x

www.rsc.org/

Hydrogen uptake during mechanochemistry of lithium nitride under 9 MPa of hydrogen pressure has been analyzed by means of *in situ* solid-gas absorption and *ex situ* X-Ray Diffraction (XRD) measurements. *In situ* hydrogenation curves show two H-sorption steps leading to an overall hydrogen uptake of 9.8wt.% H after 3 hours of milling. The milled end-products consist of nanocrystalline (~ 10 nm) LiNH₂ and LiH phases. The first reaction step comprises the transformation of polymorph α -Li₃N (S.G.P6/mmm) into β -Li₃N (S.G.P6₃/mmc) metastable phase and the reaction of the latter with hydrogen to form lithium imide: β -Li₃N + H₂ → Li₂NH + LiH. Reaction kinetics of the first step is zero-order. Its rate-limiting control is assigned to the collision frequency between milling balls and Li₃N powder. In the second absorption step, lithium imide converts to lithium amide following the reaction scheme Li₂NH + H₂ → LiNH₂ + LiH. Reaction kinetics is here limited by one-dimensional nucleation and growth mechanism which, at the light of structural data, is assigned to the occurrence of lithium vacancies in the imide compound. This study provides new insights on the reaction paths and chemical kinetics of light hydrogen storage materials during their mechanochemical synthesis.

1 Introduction

The safe and efficient storage of hydrogen is widely recognized as one of the key technological challenges in the transition towards a hydrogen-based energy economy.^{1,2} Some complex metal hydrides composed of light metallic elements are considered to be suitable candidates as hydrogen storage materials.^{3–5} Among them, the lithium imide/amide system is considered as one of the most promising hydrogen storage system due to its high hydrogen capacity and partial reversibility at moderate temperatures.^{6,7} Chen *et al.* have reported that Li₃N absorbs hydrogen using the conventional solid-gas thermally driven route.⁸ It is a stepwise reaction that entails the consecutive formation of lithium imide (Li₂NH) and lithium amide (LiNH₂)



with and overall reaction heat of - 81 kJ mol⁻¹H₂.⁸ At each step, one mol of lithium hydride (LiH) is formed. The total amount of hydrogen in the fully hydrogenated state reaches 10.4wt.% H. The first reaction step is highly exothermic (~ - 95 kJ mol⁻¹H₂)⁸ and therefore its reversibility requires high temperatures. In contrast, the second reaction step is moderately exothermic (- 66 kJ mol⁻¹H₂) leading to ~ 0.1 MPa equilibrium pressure at

250 °C.^{8,9} Thus, lithium imide reversibly absorbs hydrogen according to reaction:



with 6.5 wt.% H storage capacity. These properties make the lithium imide/amide system an attractive media for reversible hydrogen storage.⁸

Recently, it was suggested that the hydrogenation pathway of Li₃N might be more complex than that given by Eq. 1. During the first reaction step, the formation of Li₄NH intermediate has been detected.^{10,11} As for the second reaction step, David *et al.* have also observed the formation of a series of non-stoichiometric phases with the composition Li_{2-x}NH_{1+x}. Indeed, both Li₂NH and LiNH₂ are the end members of this series with values of $x = 0$ and 1 , respectively.¹² Crivello *et al.* have confirmed the stability of Li₄NH and Li_{1.5}NH_{1.5} ($x = 0.5$) by DFT calculations.¹³

An alternative method to the conventional solid-gas thermally driven synthesis of hydrides is mechanochemistry under hydrogen gas. Milling techniques represent a versatile tool for the synthesis of various functional materials.^{14–16} In the hydrogen storage field, it allows fast synthesis of nanocrystalline hydrides due to the generation of highly reactive fresh surfaces and the enhancement of solid-state reactions induced by mechanical deformations.¹⁷ Kojima and Kawai first studied mechanochemistry of lithium nitride under hydrogen gas by ball milling of Li₃N at 1 MPa of hydrogen pressure, with a ball-to-powder weight ratio (BPR) of 28:1 and milling rotation speed of 400 rpm.¹⁸ The reported hydrogen uptake was only 5 wt.%H. *Ex situ* powder X-ray diffraction measurements showed the formation of LiNH₂ but significant amounts of the starting Li₃N and intermediate Li₂NH compounds remained. The amount of hydrogen gas in the

^a CMTR/ICMPE/CNRS-UPEC, UMR7182, 2-8 rue Henri Dunant, 94320, Thiais Cedex, France.

^b General Research Institute for Nonferrous Metals, 2 Xijiekou Wai Street, Beijing 100088, China.

†Corresponding author: Tel: +33 1 49 78 12 25, Fax: +33 1 49 78 12 03. E-mail: cuevas@icmpe.cnrs.fr.

Electronic Supplementary Information (ESI) available: [XRD patterns at 15 and 30 min compared to Li₂NH, FTIR at end-of-milling, Table of refined crystallographic data]. See DOI: 10.1039/x0xx00000x

milling vial was insufficient or the BPR value too low to complete the hydrogenation reaction. Later, Minella *et al.* succeeded to accomplish the full reaction using a hydrogen pressure of 2 MPa, BPR = 75 and milling rotation speed of 550 rpm.¹⁹ However, they provided no information on the hydrogenation path and kinetic mechanisms during the mechanochemical synthesis.

In this work, the reaction pathway during mechanochemistry under hydrogen gas of Li₃N is comprehensively studied. The mechanically assisted hydrogenation reactions were monitored by *in situ* measurement of hydrogen pressure and temperature. The formation of hydride phases on milling was determined by *ex situ* X-ray diffraction measurements. Coupling between both analyses has allowed the assessment of reaction paths in this system as well as of the appraisal of the underlying reaction mechanisms.

2 Experimental procedures

Lithium nitride (Sigma-Aldrich; typical purity $\geq 99.5\%$ metal basis), and high purity hydrogen (Alphagaz; 6N) were used as starting materials. All sample handlings were done in argon filled and purified glove box. Approximately 4 g of Li₃N, 40 stainless steel balls of 12 mm in diameter and a ball-to-powder weight ratio of 80 were used for all experiments. Ball milling was performed at room temperature under initial hydrogen pressure of 9 MPa. It was conducted with a P4 Fristch Vario-Planetary mill allowing selectable rotation speeds for support disc (Ω) and milling vial (ω). In this work, the relative speed ratio between support disc and milling vial was fixed to -2 ($\Omega = 400$ rpm, $\omega = -400$ rpm). A closed-tight high pressure milling device from Evicomagnetics able to work under H₂ atmosphere up to 15 MPa was used as vial.¹⁵ *In situ* hydrogen uptake on milling was determined from pressure and corrected temperature data using the Hemmes equation.^{20,21}

Structural characterization was achieved by means of XRD using a special air tight sample holder to prevent reaction with air. XRD data was recorded with a Bruker D8 Advance

diffractometer equipped with a rear graphite monochromator. CuK $_{\alpha 1,2}$ radiation was used. The Rietveld method was employed to analyze the diffraction patterns using Fullprof software.²² The reported crystal structures for α -Li₃N,²³ β -Li₃N,²⁴ Li₂NH,²⁵ LiNH₂,²⁶ Li₄NH,²⁷ LiH,²⁸ and Li₂O¹² were used as input data. To get stable and reliable refinements, the number of refinement parameters were kept as low as possible, particularly when phase amounts were below 20 wt.%. Currently, the refined parameters were background base line, sample displacement, phase amount, lattice parameters and crystallite size. No structural parameters (atomic position, site occupation and Debye-Waller factors) were refined. The pseudo-Voigt function (number 7 for Fullprof software) was used to evaluate crystallite sizes following the procedure described in Ref.²⁹. Thermo Nicolet AVATAR 360 E.S.P. Fourier Transform Infra-Red (FTIR) spectrometer was used for complementary structural studies in the range from 3500 to 3000 cm⁻¹ in an inert atmosphere of N₂.

3 Introduction

3.1 In-situ hydrogen uptake.

Figure 1a displays the evolution of vial temperature and hydrogen pressure inside the vial as a function of milling time t . At short milling time $t < 30$ min, the vial temperature increases before equilibrating at 49 °C. Calibration experiments proved that the temperature of the hydrogen gas is *ca.* 15°C higher than the vial temperature.²⁰ As for the hydrogen pressure, it rises correlatively to the temperature for $t < 15$ min. Later on, the hydrogen pressure markedly drops indicating fast hydrogen absorption by Li₃N. After slightly more than 2 hours of milling, the hydrogen pressure reaches an equilibrium indicating that the hydrogenation reaction is completed. The trends of temperature and hydrogen pressure curves are similar to those reported by Minella *et al.*¹⁹ It is worth noting that the vial temperature is slightly higher during the pressure drop than at the end of milling, which is a signature of the exothermic nature of the hydrogenation process.

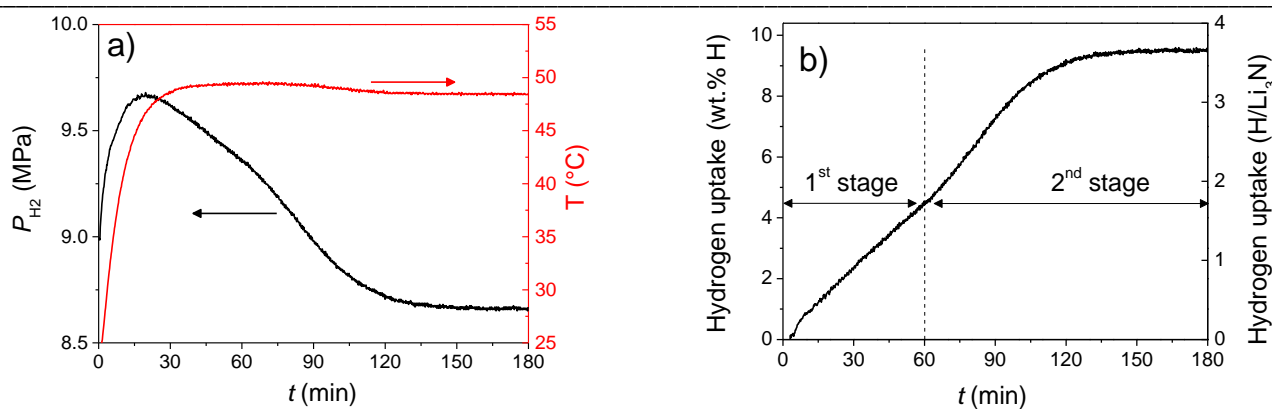


Figure 1: a) Evolution of vial temperature and hydrogen pressure during ball milling of Li₃N powder under hydrogen gas, b) Hydrogen uptake as a function of milling time.

Figure 1b shows the hydrogen uptake during milling as calculated using the procedure described in Ref. ²⁰. The total hydrogen uptake is 9.8 wt.% H, *i.e.* 3.7 equivalents of hydrogen per formula unit (H/f.u.). This represents a yield of 94 % as compared to the theoretical capacity of the $\text{Li}_3\text{N-H}$ system. The H-uptake kinetic curve can be described in two stages: it increases linearly with time for $t < 60$ min, then it follows a sigmoidal curve for longer milling times. To evidence the reactions taking place at each hydrogenation stage, *ex situ* XRD measurements were carried out.

3.2 Structural analysis of the mechanochemical process.

3.2.1 The first reaction stage.

XRD diffraction patterns were collected for $t = 0, 15, 30$ and 60 min. Figure 2 displays the graphical output of the Rietveld analysis for the four samples. All refined data are provided in ESI (Table S1). The diffraction pattern of the pristine Li_3N material (Figure 2a) can be indexed with $\alpha\text{-Li}_3\text{N}$ (S.G. $P6/mmm$, 51 wt.%)

and $\beta\text{-Li}_3\text{N}$ (S.G. $P6_3/mmc$, 44 wt.%) polymorphs. The $\beta\text{-Li}_3\text{N}$ phase corresponds to a metastable high-pressure phase.²⁴ In addition, minor amount of Li_2O (5 ± 1 wt.%) was detected. Same amount of Li_2O was observed for all samples analysed in this study, as well as by other authors using such commercial compound.³⁰ Therefore, it is likely to be an impurity present in the pristine material and its occurrence will not be further discussed in this manuscript. At $t = 15$ min (Figure 2b), no diffraction peaks from $\alpha\text{-Li}_3\text{N}$ are detected, those from $\beta\text{-Li}_3\text{N}$ increase in intensity, and new phases indexed as Li_2NH and LiH appear. On further milling (Figure 2c), the intensity of the diffraction peaks of $\beta\text{-Li}_3\text{N}$ decreases, whereas it increases for Li_2NH and LiH . No hints of the occurrence of the intermediate phase Li_4NH were observed (see Fig. S1 in ESI). At the end of this first stage ($t = 60$ min, Figure 2d), the sample contains Li_2NH (77 wt.%) and LiH (19 wt.%).

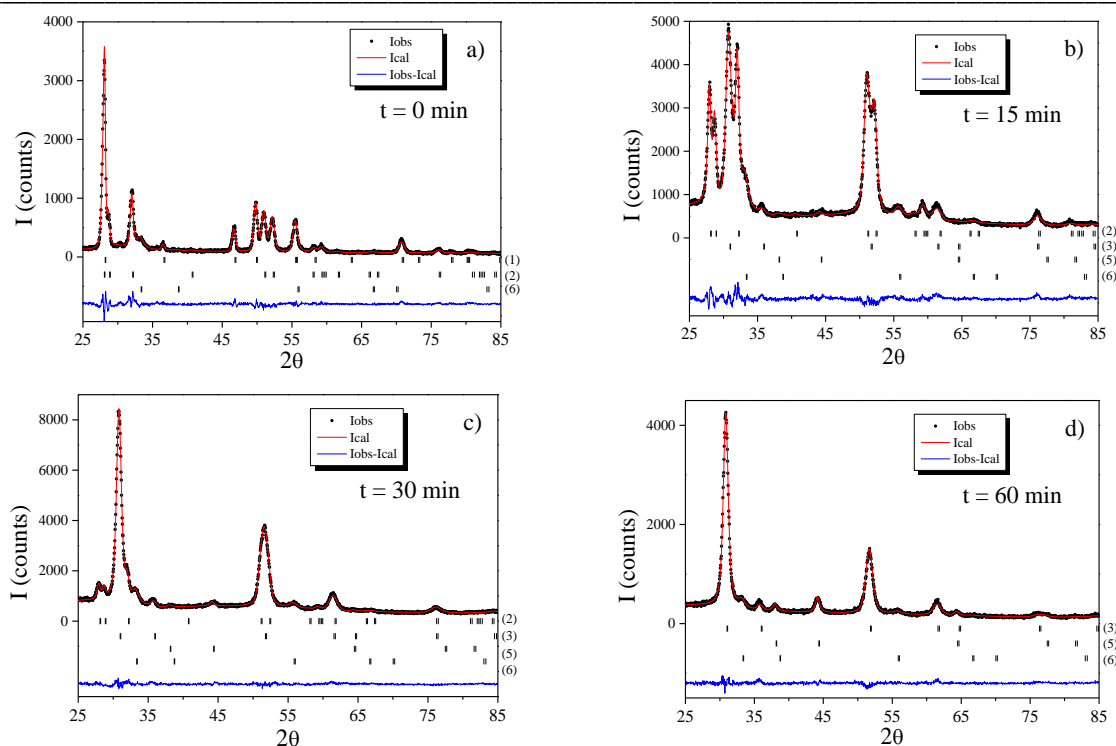


Figure 2: Rietveld analysis of XRD data collected within the first reaction stage: a), b), c), and d) stand for $t = 0, 15, 30$ and 60 min, respectively. Observed (dots), calculated (black solid line) and difference curves (blue solid line below) are shown. Vertical bars correspond to (hkl) Bragg line positions for (1) $\alpha\text{-Li}_3\text{N}$, (2) $\beta\text{-Li}_3\text{N}$, (3) Li_2NH , (4) LiNH_2 , (5) LiH and (6) Li_2O phases. Phase (4) was not detected.

3.2.2 The second reaction stage.

To analyze the reactions occurring at this stage, XRD diffraction patterns were collected for $t = 90, 120$ and 180 min. The corresponding graphical outputs for Rietveld refinement are displayed in Figure 3. Obtained data results are given in ESI (Table S1). At $t = 90$ min (Fig. 3a), new diffraction peaks belonging to LiNH_2 appeared, whereas the intensity of Li_2NH diffraction peaks decreased. Same trend was observed on further milling (Figs. 3b and 3c) with a gradual increase of the LiH diffraction peak intensities. At the end of this stage ($t = 180$ min, Figure 3c), no more lithium imide was detected and the sample was found to contain LiNH_2 (50 wt.%) and LiH (46 wt.%). The formation of LiNH_2 phase was corroborated by FTIR (ESI Fig. S2), showing the characteristic N-H symmetric and asymmetric stretching vibrations of LiNH_2 at 3258 cm^{-1} and 3312 cm^{-1} , respectively.³¹ Therefore, in the second stage, lithium imide reacts with hydrogen to form lithium amide and lithium hydride.

3.2.3 Global reaction path.

The complete reaction path during the mechanochemical process can be comprehensively visualized by plotting phase amounts as a function of milling time (Figure 4). First, $\alpha\text{-Li}_3\text{N}$ converts to $\beta\text{-Li}_3\text{N}$ at the early stage of the mechanochemical process ($t < 15$ min). Then, $\beta\text{-Li}_3\text{N}$ reacts with hydrogen following the reaction scheme:



Finally, lithium imide reacts with hydrogen according to:

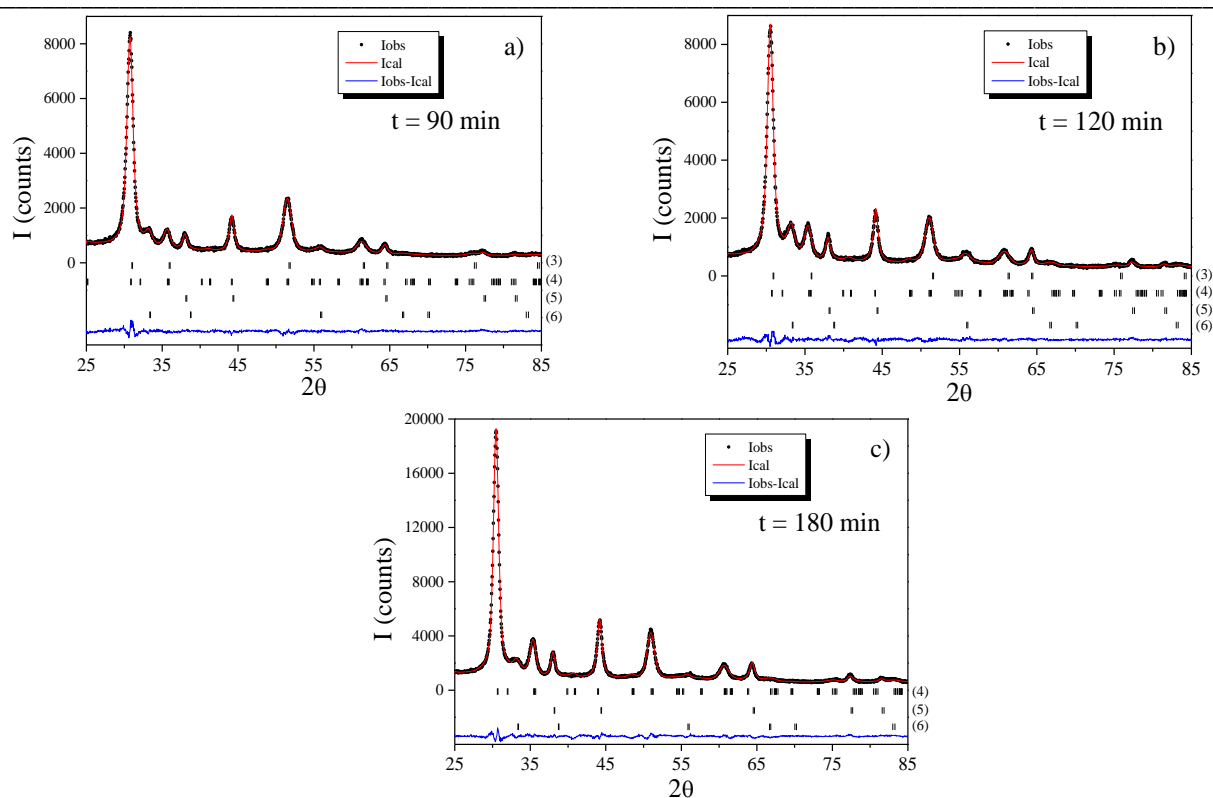


Figure 3: Rietveld analysis of XRD data collected within the second reaction stage: a), b), and c) stand for $t = 90, 120,$ and 180 min, respectively. Observed (dots), calculated (black solid line) and difference curves (blue solid line below) are shown. Vertical bars correspond to (hkl) Bragg line positions for (1) $\alpha\text{-Li}_3\text{N}$, (2) $\beta\text{-Li}_3\text{N}$, (3) Li_2NH , (4) LiNH_2 , (5) LiH and (6) Li_2O phases. Phases (1) and (2) were not detected.

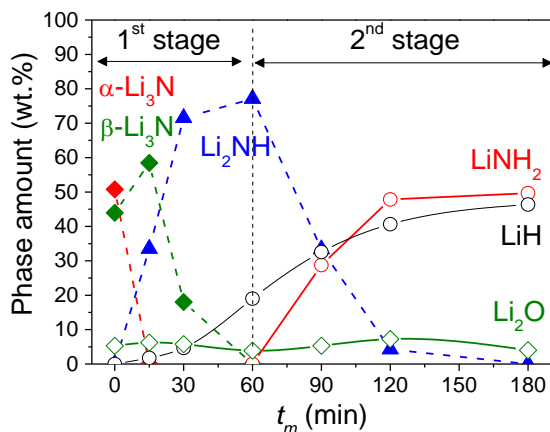


Figure 4: Evolution of phase amounts during ball milling of Li_3N powder under hydrogen gas

Each of these reactions involves the absorption of two equivalents of hydrogen per Li_3N , which matches fairly well with the monitored H-uptake at each step: 1.7 and 2 H/f.u. for the first and second step, respectively. One can note that the phase amounts of the reaction products determined in sections 3a and 3b match fairly well with the theoretical values given in Eqs. 3 and 4.

No intermediate phases such as Li_4NH and $\text{Li}_{1.5}\text{NH}_{1.5}$ for the first and second absorption stages, respectively, were detected as distinct diffraction peaks. However, the occurrence of $\text{Li}_{2-x}\text{NH}_{1+x}$ -type phases cannot be ruled out as discussed in the next section.

4 Discussion

Three different reactions have been detected during the mechanochemistry of Li_3N under hydrogen gas: *i*) the solid-state polymorphic transformation of $\alpha\text{-Li}_3\text{N}$ into $\beta\text{-Li}_3\text{N}$ at the early stage of milling, *ii*) the solid-gas reaction between $\beta\text{-Li}_3\text{N}$ and hydrogen to form Li_2NH and LiH at $t < 60$ min and *iii*) the solid-gas reaction between Li_2NH and hydrogen to form LiNH_2 and LiH at $60 < t < 180$ min.

The first reaction does not involve any H-absorption and therefore no information on its reaction mechanism can be extracted from the H-uptake kinetic curve. In particular, we cannot state whether the polymorphic transition precedes H-absorption (implying that H-kinetics are much faster for β than for $\alpha\text{-Li}_3\text{N}$ polymorph) or if both solid-state transformation and solid/gas reaction occur simultaneously. Indeed, contradictory results on the possible influence of polymorphism on the

hydrogenation properties of Li_3N can be found in the literature.^{19,32}

It is here worth mentioning outcomes from previous works on ball milling of Li_3N under inert atmosphere. In particular, Li *et al.* have shown that $\alpha\text{-Li}_3\text{N}$ can be fully converted to $\beta\text{-Li}_3\text{N}$ after 2 hours of milling.³³ The polymorph $\beta\text{-Li}_3\text{N}$ is stable at pressures over 0.6 GPa.²⁴ Such mechanical pressures could be locally achieved at impact regions on milling. Further evidence of this is, for instance, the partial formation of high pressure $\gamma\text{-MgH}_2$ polymorph (stable phase at $P > 2\text{GPa}$ ³⁴) on prolonged mechanical milling of magnesium hydride.³⁵ The transformation of α to $\beta\text{-Li}_3\text{N}$ polymorph occurs in our work in less than 15 min, *i.e.* at shorter time than previously reported on milling under inert atmosphere.³³ This suggests that milling under hydrogen may accelerate the polymorphic transformation.

The hydrogenation mechanisms for the two solid/gas reactions (Eqs. 3 and 4) can be analyzed from the shape of the H-uptake kinetic curve (Fig. 1b). For that, the method proposed by Hancock and Sharp has been adopted.³⁶ This method is valid for the kinetic analysis of isothermal solid-state reactions, including gas ab(des)orption processes in bulk. Isothermal conditions are fulfilled in our study during H-uptake (Fig. 1a), except for short reaction time, $t < 30$ min. In practical terms, linear plots of the type $\ln(-\ln(1-f))$ vs $\ln(t)$ are evaluated, being f the reacted fraction and t the reacted time. The slope of this plot, m , allows determining the rate controlling step of the reaction according to tabulated values. To our knowledge, this is the first attempt to use this approach for analyzing the reaction kinetics of hydrogen absorption during mechanical milling under hydrogen gas.

Figure 5 displays the kinetic analysis for the two reaction stages corresponding to the formation of imide (Eq. 3, Fig. 5a) and amide (Eq.4, Fig. 5b), respectively. For the second stage, the zero-time of the analysis was chosen to be at $t = 60$ min, *i.e.* at the beginning of amide formation according to the structural results (Fig. 4). As shown in Fig. 5, kinetic data can be well fitted with linear plots ($R > 0.99$) over a wide f range, from which m values of 1.21 and 1.50 are obtained for the first and second stages, respectively. It indicates a zero-order reaction for the first stage (ideally $m = 1.25$ ³⁶) and one-dimensional nucleation and growth for the later one (ideally $m = 1.50$ ³⁷).

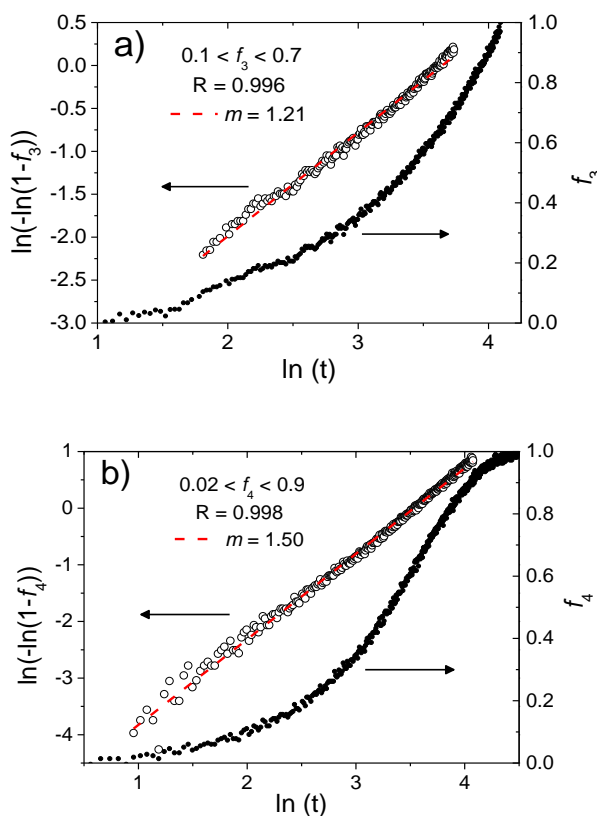
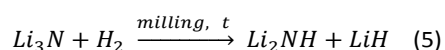


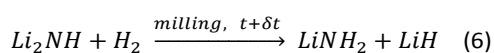
Figure 5: Kinetic analysis of Li_3N hydrogenation during the mechanochemical process: a) first reaction stage, b) second reaction stage.

Concerning the first stage, zero-order reactions are usually observed when the reaction rate does not depend on the reactant concentration.³⁸ This occurs if a limited fraction of the reactants is in a state or location in which they are able to react, and this fraction renews continuously over time. This situation clearly applies for the small fraction of Li_3N powder that at a given time endures mechanical impact between milling balls. Such a fraction would be continuously renewed as Li_3N powder moves inside the vial due to the planetary movement. Under these circumstances, one can expect that the reaction rate depends on the collision frequency between balls and Li_3N powder. On milling at fixed rotation speed, the collision frequency is constant, leading to a linear reaction rate as already anticipated in Fig. 1b.

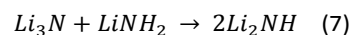
The previous mechanism states that Li_3N hydrogenation only occurs at impact location according to the reaction scheme:



One may then argue that when the so formed lithium imide experiences subsequent mechanical collisions, it should result in lithium amide formation by the analogous reaction scheme:



However, XRD data shows that LiNH_2 formation is not observed within the first stage. In other words, Li_3N is observed to fully convert into Li_2NH before starting LiNH_2 formation in the second stage. This apparent contradiction can be solved if one considers that the simultaneous coexistence of Li_3N and LiNH_2 is thermodynamically unstable as compared to the formation of Li_2NH . Such instability should trigger the following reaction scheme:



We cannot exclude that the intricate reaction mechanism provided by Eqs. 5 to 7 would be also at the origin of the observed zero-order kinetics.

At this point, it is also worth commenting on the evolution of crystallite size of the detected phases during the mechanochemical process. This information was obtained from Rietveld fits of XRD data and is shown in Fig. 6. The crystallite size of α and β -phases in the pristine Li_3N powder is evaluated as 43 ± 8 and 23 ± 2 nm, respectively. On milling, the crystallite size of β - Li_3N phase gradually decreases to a lower nanometric scale (15 ± 2 nm) for $t \leq 30$ min. Next, the crystallite size reaches a minimum and stationary size of 10 ± 2 nm for all produced phases. Thus, one can notice that crystallite size reduction occurs exclusively during the first reaction stage. The hydrogenation reaction is thought to proceed at collision location (*i.e.* milling balls/ $\text{Li}_3\text{N}/\text{H}_2(\text{g})$ interfaces) and results in increased number of solid phases in the products (Li_2NH and LiH) as compared to the unique solid reactant Li_3N favoring reduction in crystallite size. Next, on the second reaction stage equal number of reactant and product phases are involved and crystallite sizes remain constant. Further reduction in crystallite size is not observed for the conditions of mechanical energy used in this work.

The diminution in crystallite size as well as the generation of fresh surfaces undoubtedly enhance the hydrogen uptake kinetics. In addition, as demonstrated by other authors, the increase in specific surface area during milling may also play a significant role on the reaction kinetics of this system.^{39,40}

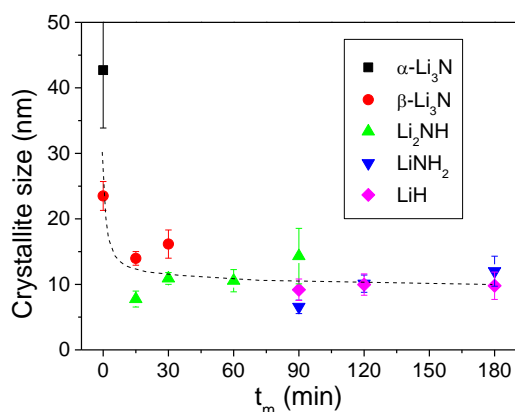


Figure 6: Crystallite sizes of the detected phases during ball milling of Li_3N powder under hydrogen gas. The dashed line is a guide for the eyes.

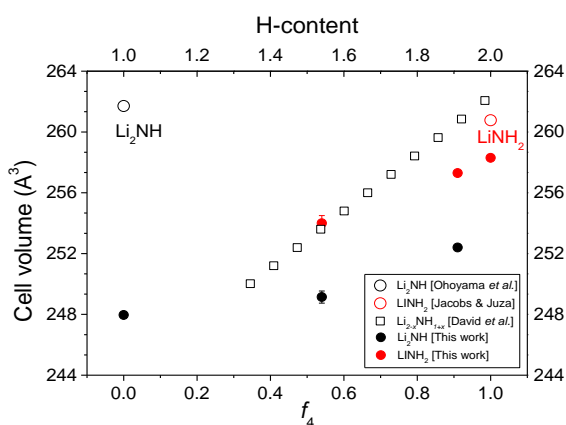


Figure 7: Cell volume variations of Li_2NH (full black circles) and LiNH_2 (red black circles) as a function of the reacted fraction (corresponding to Eq. 4). Data from this work are compared to Li_2NH ²⁵ (open black circle) and LiNH_2 ⁴¹ (open red circle) as well as mixed $\text{Li}_{2-x}\text{NH}_{1+x}$ imide/amide¹² (open squares). The unit-cell volume of the imide phase has been doubled to entail equivalent number of formula units per cell. Hydrogen content between pure imide and amide phases are assumed to be directly related to the reaction fraction corresponding to Eq. 4.

Concerning the second reaction stage, several facts deserve discussion. As already mentioned, reaction kinetics are faster than for the first stage (Fig. 1b). This observation concurs with the lower crystallinity of the involved phases, which facilitate hydrogen transfer within the bulk powder. One can argue that on decreasing crystallite sizes a change in the reaction mechanism is promoted which now entails low dimensional nucleation and growth of lithium amide from lithium imide (Fig. 5b). David *et al.* have proposed that the thermally-driven hydrogenation of lithium imide into lithium amide occurs

through a Li^+ -vacancy mediated mechanism which is evidenced by the formation of a continuous series of nonstoichiometric imide-like phases with the composition $\text{Li}_{2-x}\text{NH}_{1+x}$. To ascertain whether these phases are formed during the mechanochemistry process, we regarded in detail the evolution of the cell volumes of the imide and amide phases on milling.

Fig. 7 shows the refined cell volume of Li_2NH and LiNH_2 phases during the second stage of mechanochemistry as a function of the reacted fraction f . Experimental data from this work are compared to the reported cell volumes of Li_2NH ²⁵ and LiNH_2 ⁴¹ as well as those of the nonstoichiometric $\text{Li}_{2-x}\text{NH}_{1+x}$ imide-like phases detected by David *et al.* in H-cycled Li_3N .¹² Despite their difference in composition, cell volumes of pure Li_2NH (doubled for comparison purposes) and LiNH_2 compounds are almost the same (open circles in Fig. 7). In contrast, cell volumes of $\text{Li}_{2-x}\text{NH}_{1+x}$ gradually decrease on increasing Li-content (*i.e.* during the correlated decrease of H-content that fulfils charge balance constrains). This implies that the structural properties of nonstoichiometric $\text{Li}_{2-x}\text{NH}_{1+x}$ do not follow a simple continuous solid-solution behavior between Li_2NH and LiNH_2 but likely involve a disorder/order transition at low H-contents. Indeed, $[\text{NH}]^{2-}$ anions are disordered in lithium imide whereas $[\text{NH}_2]^-$ anions are structurally ordered in lithium amide. As for the mixed $\text{Li}_{2-x}\text{NH}_{1+x}$ imide/amide compounds, which are reported to crystallize in the lithium imide structure, DFT calculations for $x = 0.5$ showed ordering of Li vacancies as well as $[\text{NH}_2]^-$ and $[\text{NH}]^{2-}$ anions.^{12,13} Such ordering seems to be at the origin of the reduced cell-volume of mixed compounds as compared to the disordered Li_2NH compound.⁴² One can clearly notice that the cell-volume of Li_2NH and LiNH_2 detected during our mechanochemical study are much smaller than the pure compounds and compatible with those reported for the nonstoichiometric $\text{Li}_{2-x}\text{NH}_{1+x}$ phases. This confirms the occurrence of $\text{Li}_{2-x}\text{NH}_{1+x}$ phases during mechanochemical transformation from Li_2NH to LiNH_2 under hydrogen gas and supports the hypothesis of a Li-vacancy mediated mechanism in the reaction kinetics.

Conclusions

Full conversion of Li_3N into LiNH_2 and LiH has been successfully achieved in less than 3 hours by mechanochemistry under hydrogen gas. The reaction path essentially follows the same reaction scheme than for the thermally driven process though the formation of the intermediate Li_4NH phase is not observed. The overall reaction entails two major steps: the formation of lithium imide and lithium amide, both leading to steady production of LiH . The hydrogenation kinetics of the first and second steps are limited by mechanical collisions and by one-dimensional nucleation and growth of lithium amide, respectively. The second reaction step involves the formation of $\text{Li}_{2-x}\text{NH}_{1+x}$ phases suggesting the existence of a Li-vacancy mediated mechanism during hydrogen uptake.

This work confirms that mechanochemistry under hydrogen gas is an efficient technique for the synthesis of nanostructured hydrides with relevant importance for hydrogen storage.

Moreover, thanks to the complementary information provided by the kinetic analysis of *in situ* H-uptake and the structural analysis of *ex situ* diffraction data, the identification of reaction paths and the assessment of the underlying hydrogenation mechanisms are unveiled. This novel combined approach gives new light on the understanding of mechanochemical processes in the field of hydrogen storage.

Acknowledgements

The authors thank R. Janot from LRCS/CNRS (France) for FTIR measurements. Financial support of European COST action MP1103 and Egide (France) is gratefully acknowledged.

References

- 1 G. Crabtree, M. Dresselhaus and M. Buchanan, *Phys. Today*, 2004, **57**, 39–44.
- 2 L. Zhou, *Renew. Sustain. Energy Rev.*, 2005, **9**, 395–408.
- 3 J. Yang, A. Sudik, D. J. Siegel, D. Halliday, A. Drews, R. O. Carter, C. Wolverton, G. J. Lewis, J. W. A. Sachtler, J. J. Low, S. A. Faheem, D. A. Lesch and V. Ozolinš, *Angew. Chem. Int. Ed.*, 2008, **47**, 882–887.
- 4 A. W. C. van den Berg and C. O. Areal, *Chem. Commun.*, 2008, 668–681.
- 5 M. Raju and S. Kumar, *Int. J. Hydrog. Energy*, 2011, **36**, 1578–1591.
- 6 S. Srinivasan, *J. Electrochem. Soc.*, 1989, **136**, 41C–48C.
- 7 O. Palumbo, A. Paolone, R. Cantelli and D. Chandra, *Int. J. Hydrog. Energy*, 2008, **33**, 3107–3110.
- 8 P. Chen, Z. Xiong, J. Luo, J. Lin and K. L. Tan, *Nature*, 2002, **420**, 302–304.
- 9 Y. Kojima and Y. Kawai, *J. Alloys Compd.*, 2005, **395**, 236–239.
- 10 E. Weidner, D. J. Bull, I. L. Shabalin, S. G. Keens, M. T. F. Telling and D. K. Ross, *Chem. Phys. Lett.*, 2007, **444**, 76–79.
- 11 D. J. Bull, N. Sorbie, G. Baldissin, D. Moser, M. T. F. Telling, R. I. Smith, D. H. Gregory and D. K. Ross, *Faraday Discuss.*, 2011, **151**, 263–270.
- 12 W. I. F. David, M. O. Jones, D. H. Gregory, C. M. Jewell, S. R. Johnson, A. Walton and P. P. Edwards, *J. Am. Chem. Soc.*, 2007, **129**, 1594–1601.
- 13 J.-C. Crivello, M. Gupta, R. Cerný, M. Latroche and D. Chandra, *Phys. Rev. B*, 2010, **81**, 104113–11.
- 14 O. Gutfleisch, M. Kubis, A. Handstein, K.-H. Müller and L. Schultz, *Appl. Phys. Lett.*, 1998, **73**, 3001–3003.
- 15 S. Doppiu, L. Schultz and O. Gutfleisch, *J. Alloy Compd.*, 2007, **427**, 204–208.
- 16 C. Suryanarayana, *Prog. Mater. Sci.*, 2010, **46**, 1–184.
- 17 J. Huot, D. B. Ravnsbæk, J. Zhang, F. Cuevas, M. Latroche and T. R. Jensen, *Prog. Mater. Sci.*, 2013, **58**, 30–75.
- 18 Y. Kojima, Y. Kawai and N. Ohba, *J. Power Sources*, 2006, **159**, 81–87.
- 19 C. B. Minella, C. Rongeat, R. Domènech-Ferrer, I. Lindemann, L. Dunsch, N. Sorbie, D. H. Gregory and O. Gutfleisch, *Faraday Discuss.*, 2011, **151**, 253–262.
- 20 J. Zhang, F. Cuevas, W. Zaïdi, J.-P. Bonnet, L. Aymard, J.-L. Bobet and M. Latroche, *J. Phys. Chem. C*, 2011, **115**, 4971–4979.
- 21 H. Hemmes, A. Driessen and R. Griessen, *J. Phys. C Solid State Phys.*, 1986, **19**, 3571–3585.
- 22 J. Rodríguez-Carvajal, *Phys. B*, 1993, **192**, 55–69.
- 23 D. H. Gregory, P. M. O'meara, A. G. Gordon, J. P. Hodges, S. Short and J. D. Jorgensen, *Chem. Mater.*, 2002, **14**, 2063–2070.
- 24 H. J. Beister, S. Haag, R. Kniep, K. Strössner and K. Syassen, *Angew. Chem. Int. Ed. Engl.*, 1988, **27**, 1101–1103.
- 25 K. Ohoyama, Y. Nakamori, S. Orimo and K. Yamada, *J. Phys. Soc. Jpn.*, 2005, **74**, 483–487.
- 26 M. H. Sørby, Y. Nakamura, H. W. Brinks, T. Ichikawa, S. Hino, H. Fujii and B. C. Hauback, *J. Alloys Compd.*, 2007, **428**, 297–301.
- 27 R. Niewa and D. A. Zherebtsov, *Z. Für Krist. New Cryst. Struct.*, 2002, **217**, 317–318.
- 28 R. S. Calder, W. Cochran, D. Griffiths and R. D. Lowde, *J. Phys. Chem. Solids*, 1962, **23**, 621–632.
- 29 J. R. Ares, F. Cuevas and A. Percheron-Guegan, *Acta Mater.*, 2005, **53**, 2157–2167.
- 30 J. Lamb, D. Chandra and W.-M. Chien, *J. Phys. Chem. C*, 2011, **115**, 14386–14391.
- 31 J.-P. O. Bohger, R. R. Eßmann and H. Jacobs, *J. Mol. Struct.*, 1995, **348**, 325–328.
- 32 A. Huq, J. W. Richardson, E. R. Maxey, D. Chandra and W.-M. Chien, *J. Alloys Compd.*, 2007, **436**, 256–260.
- 33 W. Li, G. Wu, C. M. Araújo, R. H. Scheicher, A. Blomqvist, R. Ahuja, Z. Xiong, Y. Feng and P. Chen, *Energy Environ. Sci.*, 2010, **3**, 1524–1530.
- 34 M. Bortz, B. Bertheville, G. Böttger and K. Yvon, *J. Alloys Compd.*, 20101120, **287**, L4–L6.
- 35 J. Huot, I. Swainson and R. Schulz, *Ann. Chim.-Sci. Mater.*, 2006, **31**, 135–144.
- 36 J. D. Hancock and J. H. Sharp, *J. Am. Ceram. Soc.*, 1972, **55**, 74–77.
- 37 J. E. House, *Principles of chemical kinetics*, Elsevier/Academic Press, Amsterdam; Boston, 2007.
- 38 R. H. Petrucci, *General chemistry: principles and modern applications*, Pearson Canada, Toronto, Ont., 2011.
- 39 T. Markmaitree, R. Ren and L. L. Shaw, *J. Phys. Chem. B*, 2006, **110**, 20710–20718.
- 40 R. A. Varin, M. Jang and M. Polanski, *J. Alloys Compd.*, 2010, **491**, 658–667.
- 41 H. Jacobs and R. Juza, *Z. Für Anorg. Allg. Chem.*, 1972, **391**, 271–279.
- 42 M.-L. Bonnet, M. Iannuzzi, D. Sebastiani and J. Hutter, *J. Phys. Chem. C*, 2012, **116**, 18577–18583.